



HAL
open science

Pks5-recombination-mediated surface remodelling in Mycobacterium tuberculosis emergence

Eva C. Boritsch, Wafa Frigui, Alessandro Cascioferro, Wladimir Malaga,
Gilles Etienne, Françoise Laval, Alexandre Pawlik, Fabien Le Chevalier,
Mickael Orgeur, Laurence Ma, et al.

► **To cite this version:**

Eva C. Boritsch, Wafa Frigui, Alessandro Cascioferro, Wladimir Malaga, Gilles Etienne, et al.. Pks5-recombination-mediated surface remodelling in Mycobacterium tuberculosis emergence. *Nature Microbiology*, 2016, 1 (février 2016), 10.1038/nmicrobiol.2015.19 . pasteur-01265519

HAL Id: pasteur-01265519

<https://pasteur.hal.science/pasteur-01265519>

Submitted on 1 Feb 2016

HAL is a multi-disciplinary open access archive for the deposit and dissemination of scientific research documents, whether they are published or not. The documents may come from teaching and research institutions in France or abroad, or from public or private research centers.

L'archive ouverte pluridisciplinaire **HAL**, est destinée au dépôt et à la diffusion de documents scientifiques de niveau recherche, publiés ou non, émanant des établissements d'enseignement et de recherche français ou étrangers, des laboratoires publics ou privés.



Distributed under a Creative Commons Attribution - NonCommercial - NoDerivatives 4.0
International License

1 ***pks5*-recombination-mediated surface remodelling in *Mycobacterium tuberculosis***
2 **emergence**

3

4 Eva C. Boritsch¹, Wafa Frigui¹, Alessandro Cascioferro¹, Wladimir Malaga^{2,3}, Gilles
5 Etienne^{2,3}, Françoise Laval^{2,3}, Alexandre Pawlik¹, Fabien Le Chevalier^{1,5}, Mickael Orgeur¹,
6 Laurence Ma⁴, Christiane Bouchier⁴, Timothy P. Stinear⁶, Philip Supply⁷, Laleh Majlessi¹,
7 Mamadou Daffé^{2,3}, Christophe Guilhot^{2,3,*} and Roland Brosch^{1,*}.

8

9 ¹Institut Pasteur, Unit for Integrated Mycobacterial Pathogenomics, 75015 Paris, France;

10 ²CNRS, IPBS (Institut de Pharmacologie et de Biologie Structurale), 31000 Toulouse, France;

11 ³Université de Toulouse, UPS, IPBS, 31000 Toulouse, France;

12 ⁴Institut Pasteur, PF1-Plate-Forme Génomique, Paris, France;

13 ⁵University Paris Diderot, Sorbonne Paris Cité, Cellule Pasteur, Paris, France

14 ⁶Department of Microbiology and Immunology, University of Melbourne, Parkville,
15 Victoria, Australia.

16 ⁷Inserm U1019, CNRS UMR8204, Université de Lille, Institut Pasteur de Lille, Center for
17 Infection and Immunity, 59000 Lille, France.

18

19 *Corresponding authors: Christophe.Guilhot@ipbs.fr and roland.brosch@pasteur.fr

20

21 *Mycobacterium tuberculosis* is a major, globally spread, aerosol-transmitted human pathogen,
22 thought to have evolved by clonal expansion from a *Mycobacterium canettii*-like progenitor.
23 In contrast, extant *M. canettii* strains are rare, genetically diverse and geographically
24 restricted mycobacteria of only marginal epidemiological importance. Here we show that the
25 contrasting evolutionary success of these two groups is linked to loss of lipooligosaccharide
26 (LOS) biosynthesis and subsequent morphotype changes. Spontaneous smooth-to-rough *M.*
27 *canettii* variants were found mutated in the polyketide-synthase-encoding *pks5* locus and
28 deficient in LOS synthesis; a phenotype restored by complementation. Importantly, these
29 rough variants showed altered host-pathogen interaction and increased virulence in cellular-
30 and animal-infection models. In one variant, LOS deficiency occurred via homologous
31 recombination between two *pks5* copies and removal of the intervening acyltransferase-
32 encoding gene. The resulting single *pks5* configuration is similar to that fixed in *M.*
33 *tuberculosis*, known to lack LOS. Our results suggest that *pks5*-recombination-mediated
34 bacterial surface remodelling increased virulence, driving evolution from putative generalist
35 mycobacteria towards professional pathogens of mammalian hosts.

36 Tuberculosis is a major human infectious disease. Although many aspects of the disease-
37 causing potential of its etiological agent *Mycobacterium tuberculosis* are known¹, our
38 understanding is scant of the molecular events that favoured its evolutionary success as one of
39 the most widely distributed human pathogens. New insights into this question are important
40 for uncovering mechanisms of pathogenesis and new drug targets². Strains of the closely
41 related and phylogenetically early branching *Mycobacterium canettii*, also named smooth
42 tubercle bacilli (STB)³ are powerful resources to investigate the evolution of *M. tuberculosis*
43 and the *M. tuberculosis* complex (MTBC)³. The first strain of *M. canettii* was isolated by
44 Georges Canetti in 1969 and since then less than 100 isolates have been described, most of
45 which have been isolated from tuberculosis patients with a connection to the Horn of Africa⁴
46 ⁷. Despite their geographic restriction, *M. canettii* strains show much greater genetic
47 variability and are less virulent/persistent than *M. tuberculosis*. Genome comparisons suggest
48 that *M. tuberculosis* evolved by clonal expansion from a pool of *M. canettii*-like tubercle
49 bacilli through the gain of virulence and persistence mechanisms^{3,8,9}. While some genomic
50 differences were found to be specific for a single *M. canettii* strain, apparently due to isolated
51 horizontal gene transfer (e.g. the *mce5* operon³ or the *eptABCD* operon¹⁰, present exclusively
52 in strain STB-J)³, others are conserved throughout all *M. canettii* strains as a result of
53 phylogenetic ancestry (e.g. *cobF*, present in *M. canettii* and deleted from the MTBC)³.

54 Here we investigated phenotypic differences between *M. canettii* and *M. tuberculosis*
55 and focused on the unique, conserved, smooth (S) colony morphotype of *M. canettii*, as
56 opposed to the rough (R) morphotype of MTBC members. Previously, S-morphotypes of non-
57 tuberculous mycobacterial species such as *Mycobacterium avium*¹¹, *Mycobacterium*
58 *abscessus*¹², *Mycobacterium kansasii*¹³ or *Mycobacterium marinum*¹⁴ have been found to be
59 less virulent than R-morphotypes, raising the question of whether the highly conserved *M.*
60 *tuberculosis* R-morphotype might have been the result of evolutionary selection, based on
61 host-pathogen interactions favouring a more virulent or persistent phenotype. In other
62 mycobacterial species, S/R variation is often attributed to different kinds of cell surface
63 glycolipids, such as glycopeptidolipids (GPL) for *M. avium*¹⁵ and *M. abscessus*^{16,17} or
64 lipooligosaccharides (LOS) for *M. kansasii*¹³ and *M. marinum*^{14,18,19}. Insights from earlier
65 studies for *M. canettii* have remained abstruse as no specific lipid exclusively present in the S-
66 morphotype has been identified²⁰, nor has the genetic basis for morphotype variation been
67 determined⁴.

68 Building on recent data from several *M. canettii* genomes³, here we studied smooth
69 and spontaneously converted R-variants of two different *M. canettii* strains, STB-K (CIPT

70 140070010) and STB-I (CIPT 140070007)³, hereafter named K_{S/R} and I_{S/R}, respectively. We
71 used whole genome sequencing (WGS) and identified differences in genes of the *pks5* locus,
72 which in *Mycobacterium smegmatis*, *M. marinum* or *M. kansasii* are implicated in LOS
73 biosynthesis^{14,21-23}. In this report we uncover the mechanisms underlying the S-to-R
74 morphology change of tubercle bacilli and explore the biological consequences with emphasis
75 on the patho-evolution of *M. tuberculosis*.

76

77 **RESULTS**

78 **Genome comparison of *M. canettii* S- and R-variants**

79 During passaging of different smooth *M. canettii* strains, we observed spontaneous R-
80 morphotype variants for two *M. canettii* strains (I and K). These R-variants were re-passaged
81 three times on solid medium to ensure stable phenotypes and subjected to Illumina-based
82 WGS. The results obtained pointed to morphotype-linked alterations in the *pks5* locus of *M.*
83 *canettii* S/R variants (Supplementary Tables 1 and 2, Supplementary Note), which was of
84 particular interest given suggested roles for Pks5 polyketide synthases in morphotype changes
85 and LOS production in different mycobacterial species^{14,21}. In the LOS-producers *M.*
86 *marinum*²⁴ and *M. kansasii*²⁵, the Pks5-encoding locus harbours two proximal *pks5* homologs
87 separated by one or more interspaced *pks5*-associated gene(s) (Fig. 1A). The genome of *M.*
88 *canettii* STB-A³ also shows a twin-*pks5* configuration similar to *M. marinum*. In contrast *M.*
89 *tuberculosis*, which does not produce LOS only has a single *pks5* and lacks a full-length *pap*
90 ortholog (Fig. 1A).

91

92 **Recombination of two *pks5* genes in *M. canettii* K_R and *M. tuberculosis***

93 To characterize the *pks5* locus in strains I_{S/R}, K_{S/R} and *M. tuberculosis* H37Rv we performed
94 long-range PCR using *pks5*-flanking primers, yielding amplicons of ca. 15 kb for both the S-
95 and R-variants of strain I, and 6 kb for *M. tuberculosis* H37Rv, corresponding to the twin- and
96 single-*pks5* configuration, respectively (Fig. 1 A, B). For strain K, however, the prevalent
97 amplicon size of the S-variant was 15 kb, while the size for the R-variant was 6 kb, which was
98 surprising because the previously released STB-K genome sequence assembly³ indicated only
99 a single *pks5*. The PCR result suggests that the previous WGS-based genome assembly of
100 strain K (NC_019951) contained a misassembly in that region probably due to high sequence
101 identity (> 94 %) between the two *pks5* genes. Similarly, we also confirmed the presence of
102 two *pks5* genes by long-range PCR amplicon-sequencing for *M. canettii* strains D and J, for
103 which previously only one *pks5* was indicated in the released genome sequences NC_019950

104 and NC_019952, respectively (Supplementary Fig. 1). Hence, the results obtained for S- and
105 R-variants of strain K suggest that K_S contains two *pks5* genes, flanking a gene (*pap*) coding
106 for a putative polyketide-synthase-associated acyltransferase²⁶, whereas K_R only harbours a
107 single *pks5* and no interspaced *pap* gene.

108 These findings were supported by results obtained by alignment to the reference
109 sequences of *M. canettii* STB-A and *M. tuberculosis* H37Rv (Supplementary Fig. 2 and
110 Supplementary Note). This analysis suggested that homologous recombination in strain K_R
111 occurred at a site that left intact the typical polyketide-synthase domain structures of Pks5^{26,27}
112 (Fig. 1). The observed *pks5* configuration in K_R can thus serve as a model for the situation
113 found in *M. tuberculosis*, where two former *pks5* genes also seem to have coalesced into a
114 single *pks5* gene. In the latter case, the proposed recombination event also left the domain
115 organisation of Pks5 intact, although the site of recombination was apparently different from
116 the site observed for K_R (Fig. 1 and Supplementary Fig. 2B). Further comparisons among
117 different MTBC members⁹ showed > 99.93% sequence identity of the single *pks5* gene in
118 these strains, suggesting a unique recombination event in the most recent common ancestor of
119 the MTBC after the separation from an *M. canettii*-like progenitor.

120 Finally, for strain I, amplicon-sequencing of the *pks5* locus of I_R and I_S confirmed the
121 presence of *pap* and two *pks5* copies in both morphotypes. However, alignment of amplicon-
122 derived sequences indicated the presence of multiple non-synonymous SNPs in both *pks5*
123 genes (6 in *pks5-2* and 3 in *pks5-1*) for the R-variant (Supplementary Fig. 3A), which likely
124 resulted from recombination of the ketosynthase domain regions of the *pks5* copies
125 (Supplementary Fig. 3B). From these data we predicted that these changes likely caused the
126 R-morphotype of I_R.

127

128 **Pap and Pks5-2 restore the S-morphotype in *M. canettii***

129 To test if changes in the *pks5* locus were responsible for the S/R variations in *M. canettii*, we
130 transformed strains K_R and I_R, as well as *M. tuberculosis* H37Rv with the integrating cosmid
131 C9, selected from an *M. canettii* STB-A large-fragment genomic library constructed for this
132 purpose in pYUB412. This vector integrates into the *attB* site located in the *glyV*-tRNA of
133 mycobacterial genomes²⁸. The 30.5 kb insert of cosmid C9 spans the *pks5* locus of STB-A
134 (Supplementary Fig. 4). Fig. 2 shows that recombinant *M. canettii* strains I_R::C9 and K_R::C9
135 regained S-morphology that was indistinguishable from their respective S-variants. To refine
136 the region required for S-morphotype restitution, we isolated a second cosmid, named H6 that
137 contains full-length *pap* and *pks5-2* but a 3'-truncated *pks5-1* (Supplementary Fig. 4).

138 Transformation of I_R and K_R with H6 yielded smooth colonies for both I_R::H6 and K_R::H6
139 (Supplementary Fig. 5A).

140 Complementation with a *pks5-2* single gene expression construct restored an S-
141 morphotype for strain I_R::*pks5-2*, but not for K_R::*pks5-2* (Supplementary Figs. 5B and 5C).
142 Moreover, transformation with *pap* was unable to restore smooth colonies in either of the
143 strains despite appropriate protein expression (Supplementary Figs. 5B and 5D). Together, the
144 complementation experiments suggest that *pks5-2* and *pap* are necessary for the S-
145 morphotype in *M. canettii*.

146 In contrast, R-morphology of *M. tuberculosis* H37Rv remained unchanged upon
147 transformation with cosmid C9 (Fig. 2A) despite correct genomic integration of the cosmid
148 (Fig. 3). Similarly, transformation of other MTBC lineage members with C9 did not yield S-
149 morphotypes (Supplementary Fig. 6). These results suggest that apart from an appropriate
150 *pks5-pap* locus, additional genes intervene in the formation of S-morphotypes in tubercle
151 bacilli.

152

153 ***M. canettii* strains synthesize LOS**

154 Analysis of total lipid extracts from a large panel of *M. canettii* strains by thin-layer
155 chromatography (TLC) showed glycoconjugate spots, with TLC mobilities similar to that of
156 LOS from *M. canettii* reference strain CIPT-140010059 (STB-A or *M. canettii* strain A)²⁹ in
157 all tested strains. Substantial differences in the quantity produced by each strain were
158 observed (Fig. 4A). In contrast, no such glycoconjugates were detected in *M. tuberculosis*
159 H37Rv, consistent with the long-standing knowledge that *M. tuberculosis* does not synthesize
160 LOS (Fig. 4A)³⁰. Purification and MALDI-TOF mass spectrometry analysis of LOS from *M.*
161 *canettii* strains A, K_S and I_S revealed pseudomolecular-ion mass peaks at *m/z* 2530, 2572, and
162 2614 for LOS from strain K_S (Fig. 4B) and strain A²⁹, whereas the pattern of strain I_S showed
163 peaks at *m/z* 2516, 2558 and 2600 (Fig. 4B), consistent with the different mobility on TLC
164 (Figs. 4A and 4C). The 14 mass-unit difference indicates strain-specific structural differences,
165 likely due to the absence of one methyl-group from the carbohydrate or the lipid moiety.

166 The structure of the simplest carbohydrate domain of the *M. canettii* LOS is 2-O-Me-
167 α-L-Fucp(1->3)-β-D-Glcp(1->3)-2-O-Me-α-L-Rhap(1->3)-2-O-Me-α-L-Rhap(1->3)-β-D-
168 Glcp(1->3)-4-O-Me-α-L-Rhap(1->3)-6-O-Me-α-D-Glc(1<->1)-tri-O-acyl-α-D-Glc (Fig. 4D).
169 This octaglycosyl unit is usually further glycosylated by an incompletely defined *N*-acyl
170 derivative of a 4-amino-4,6-dideoxy-Galp residue to generate a second nonasaccharide-
171 containing glycolipid (LOS 9) (Fig. 4D)²⁹. The MALDI-TOF mass spectra of LOS purified

172 from strains K and A are consistent with the LOS 9 structure. Of note, similar patterns of ion
173 mass peaks were detected in spectra of LOS purified from *M. canettii* strains D, E, F, G, L,
174 and H, while LOS of strain J showed a 14 mass difference, similar to strain I_S (Supplementary
175 Fig. 7).

176 **Rough *M. canettii* variants I and K are deficient in LOS biosynthesis**

177 Having established that all tested *M. canettii* strains synthesized LOS, we next compared the
178 production of these glycoconjugates in the R-variants of I and K. As predicted, I_R was
179 severely impaired in LOS production with only trace amounts detected, and LOS was
180 undetectable in K_R (Fig. 4C and Supplementary Fig. 8). No other differences in polyketide-
181 derived-lipids were observed between the S- and R-variants (Supplementary Fig. 9).
182 Complementation with cosmid C9 restored LOS biosynthesis in recombinant I and K strains
183 (Fig. 4C), whereas recombinant expression of *pks5-2* alone restored the LOS profile in
184 I_R::*pks5-2*, but not in K_R::*pks5-2* (Supplementary Fig. 10A), likely due to the absence of full-
185 length *pap* in K_R::*pks5-2*. Indeed, based on current knowledge on acyl-trehalose biosynthesis
186 in *M. tuberculosis*^{31,32}, a *pap*-encoded acyltransferase is needed to catalyze the transfer of
187 Pks-produced polymethyl-branched fatty acids onto trehalose.

188 We also tested LOS production in the MTBC strains complemented with cosmid C9,
189 despite unaffected R-morphotype. LOS was not detected in any of the recombinant *M.*
190 *tuberculosis* strains (Supplementary Fig. 10B), suggesting that apart from *pks5* recombination
191 and *pap* deletion, in the MTBC additional loss-of-function mutations or insertions/deletions
192 (indels) have occurred in adjacent genes of the LOS-encoding locus that are not covered by
193 cosmid C9 (Supplementary Tables 3 and 4). These results establish that point mutations or
194 recombination/deletion events in the core *pks5-pap* locus of *M. canettii* strains I_R and K_R led
195 to LOS deficiency and R-morphology. The results also explain the R-morphotype of *M.*
196 *tuberculosis* and open new perspectives for detailed research on the functions of *pks5*-
197 adjacent genes.

198

199 **Increased fitness and virulence of R-variants in cellular and animal models**

200 Given the identified altered cell surface structure associated with S/R morphology, the
201 question arose whether these changes had an impact on host-pathogen interactions. We thus
202 undertook a series of infection experiments, starting with tests of intracellular replication, a
203 hallmark of mycobacterial virulence. Differentiated human THP-1 macrophages were infected
204 with Sauton-grown *M. canettii* strains K_S, K_R and K_R::C9, as well as K_R::vector-control, up to

205 five days. While no intracellular growth was observed for K_S and $K_R::C9$, the R-morphotypes
206 K_R and $K_R::$ vector-control replicated readily, analogous to *M. tuberculosis* H37Rv (Figs. 5A
207 and 5B). Similar results were obtained when human peripheral blood monocyte-derived
208 macrophages from healthy donors were infected with the different morphotypes
209 (Supplementary Fig. 11A), confirming that the increased fitness advantage of the R-
210 morphotypes was a general phenomenon in human macrophages and not just in THP-1 cells.
211 For murine-derived RAW macrophages a similar trend, but without significant difference was
212 observed (Supplementary Fig. 11B).

213 To test whether an increased fitness advantage could also be observed *in vivo*, we first
214 infected SCID mice intravenously with 1×10^6 CFU of each morphotype. Mice infected with
215 *M. tuberculosis* H37Rv or *M. canettii* K_R had a median survival of 16 and 24 days pi,
216 respectively, while mice infected with strains K_S and $K_R::C9$ had a longer survival time; on
217 average 31 and 36 days, respectively (Fig. 5C). Higher virulence of R-morphotypes was also
218 observed in the sensitive guinea pig model, using low-dose aerosol infection (Fig. 5D). While
219 in this highly susceptible model, the S-variants of *M. canettii* were already substantially
220 virulent and able to replicate in infected animals, the ratios of the bacterial burden in the lungs
221 at day 42 relative to day 1 were significantly higher for strain K_R than those for the S-
222 morphotypes. Interestingly, for animals infected with $K_R::C9$ (Fig. 2) we observed more than
223 half of the colonies showing a re-converted R-morphotype, which was never observed in any
224 of our previous *in vitro* experiments, suggesting possible reversion of the usually very stable
225 pYUB412-based integrated genetic complementation³³, due to *in vivo* fitness advantages of R-
226 morphotypes during the long-duration *in vivo* infection assays.

227 To further investigate the host-pathogen interaction of S- and R-variants, we
228 characterized the inflammatory responses induced in infected phagocytes, as recently
229 performed for S- and R-forms of *M. abscessus*^{34,35}. As shown in Figs. 5E and 5F, a potential
230 LOS-dependent anti-inflammatory effect was observed in *M. canettii*-infected bone-marrow
231 derived dendritic cells (BM-DCs) of C57BL/6 mice. Strains K_S and $K_R::C9$ induced
232 significantly lower secretion of NF- κ B-dependent inflammatory cytokines IL-6 and IL-12p40
233 than K_R . Results with these two cytokines, known to be induced in response to infection with
234 *M. tuberculosis*³⁶, were also representative for TNF- α and NF- κ B-dependent CCL5 and
235 CXCL10 chemokines (Supplementary Fig. 12). In our experimental conditions, most of the
236 responses were dependent on interaction via Toll-like receptor 2 (TLR-2). Smooth variants
237 showed reduced interaction with this crucial innate immune sensor of numerous
238 mycobacterial ligands (Figs. 5 G, 5H and Supplementary Fig. 13). Presence or absence of

239 LOS thus seems to strongly influence the complex pattern of host-tubercle bacilli interaction,
240 with likely consequences for virulence and pathogenesis.

241

242 **DISCUSSION**

243 The evolutionary transition for a bacterial population from low-virulence/high genetic
244 diversity towards high-virulence/low genetic diversity is well established for some major
245 human pathogens such as *Yersinia pseudotuberculosis* vs *Yersinia pestis* or *Salmonella*
246 *enteritidis* vs *Salmonella typhi*³⁷. In contrast, the specific genetic changes that led to the
247 emergence of *M. tuberculosis* are less well understood. Here we have exploited the ancestral-
248 state characteristics of *M. canettii* to address this gap in our knowledge^{3,6,9}. We show that the
249 transition of *M. tuberculosis* from likely generalist to obligate pathogen was associated with a
250 dramatic change in mycobacterial surface glycolipid composition. The S-to-R morphotype
251 variation we have studied here has been linked with higher virulence in opportunistic
252 pathogenic mycobacteria¹¹⁻¹⁴ and variation in LOS content has been shown to account for
253 morphology differences in *M. kansasii*¹³ or *M. marinum*^{14,18,19}. However, earlier studies on *M.*
254 *canettii* colony morphology have provided inconclusive results. While a study from van
255 Soolingen and coworkers found differences in LOS content between S/R colony variants of
256 an *M. canettii* strain isolated from a 2-year-old Somali child⁴, Lemassu and colleagues did not
257 observe a correlation between LOS content and colony morphology in various strains tested²⁰,
258 likely because the used strains were poor LOS producers with intermediate morphotypes. In
259 this current work we resolve these ambiguities and clearly link LOS biosynthesis with the
260 smooth colony morphotype. We also provide a genetic mechanism for the phenotype that
261 helps explain the evolution of the tubercle bacilli. Our results indicate that recombination of
262 two *pks5* genes associated with deletion of the interspersed *pap* gene evidently was a
263 molecular event that became fixed in the most recent common ancestor of the MTBC after the
264 phylogenetic separation from the *M. canettii* clade (Fig. 6). Indeed, while *M. canettii* strains
265 possess a twin *pks5* and *pap* conformation and synthesize LOS, all members of the classical
266 MTBC contain an abridged *pks5* locus missing a full length *pap* gene and do not produce
267 LOS. Identification of a similar recombination event in a spontaneous R-variant of *M. canettii*
268 K reinforces the likelihood of this evolutionary scenario. Comparable recombination-deletion
269 events also occurred for other genes, e.g. *pknH* (Supplementary Note).

270 Pks5 is a type-I polyketide synthase and a member of the broader polyketide-synthase
271 family, which in mycobacteria have important functions that range from catalyzing the
272 essential last condensation step of mycolic acid biosynthesis (Pks13)³⁸ to the synthesis of the

273 polyketide backbone of phenolic glycolipids (Pks15/1)³⁹ or the synthesis of mycoketides
274 (Pks12)⁴⁰. In *M. marinum*, the two Pks5 polyketide synthases (Pks5 and Pks5.1) are thought
275 to be involved in the synthesis of polymethyl-branched fatty acids, which are further modified
276 by glycosyltransferases and methyltransferases encoded by genes adjacent to the *pks5*
277 genes^{22,23,41} to produce LOS. Indeed, disruption of *pks5* (*MMAR_2340*), analogous to
278 disruptions of the adjacent genes *fadD25* (*MMAR_2341*), *papA4* (*MMAR_2343*), and *papA3*
279 (*MMAR_2355*) leads to a complete loss of LOS, suggesting that besides the core *pks5-pap*
280 locus, several flanking genes are also involved in the early steps of LOS-
281 biosynthesis^{14,18,19,22,23,41,42} (Supplementary Table 3).

282 Within the group of tubercle bacilli, the overall genetic organization of the
283 orthologous LOS locus is similar between *M. canettii* and the non-functional version in *M.*
284 *tuberculosis*. However, apart from the recombined *pks5* and the deleted *pap* gene, several
285 flanking genes show SNPs and small indels (Supplementary Table 4), some of which might
286 represent loss-of-function mutations involved in the non-complementation phenotype with
287 cosmid C9 in MTBC members. These findings suggest that after the phylogenetic separation
288 of the MTBC from the *M. canettii*-like progenitor pool, in addition to *pks5* recombination and
289 *pap* deletion, other mutations in genes of the LOS locus accumulated in the MTBC in the
290 absence of selective pressure for sustaining LOS biosynthesis. While LOS production might
291 play an important role in generalist mycobacteria, it appears that its absence might provide a
292 selective advantage for specialized pathogens in the mammalian host.

293 This conclusion is supported by our different infection experiments, where loss of
294 LOS by *M. canettii* R-variants led to increased virulence in human macrophages and under *in*
295 *vivo* conditions, particularly for the sensitive guinea pig infection model. These data support a
296 scenario wherein the recombination of *pks5* genes in a common ancestor of the MTBC has
297 contributed to the evolutionary success and host adaptation of the resulting LOS-deprived
298 strains. This finding is in agreement with data for other mycobacterial species, where
299 increased virulence of R-morphotypes relative to S-morphotypes has been reported^{11,12,14},
300 although the involved glycolipids are different. In *M. avium*, for example, homologous
301 recombination within the *ser2* gene cluster likely led to phenotype changes linked to loss of
302 GPLs⁴³. For *M. abscessus*, a masking effect of GPLs on the outermost layer of the cell wall
303 of the S-morphotype strains has been suggested, which was related to repression of TLR2
304 responses³⁴. Similarly, LOS is located in the outermost layer of the mycobacterial cell
305 envelope⁴⁴ and thus might be interacting with other cell wall-associated
306 lipids/glycoconjugates such as phthiocerol dimycocerosates, lipoarabinomannans or the 19-

307 kD lipoprotein⁴⁵, which are important for host-pathogen interaction⁴⁶. At present, it is difficult
308 to speculate by which mechanisms R-variants of tubercle bacilli might have gained a fitness
309 advantage during infection. However, differences we show here in TLR2-mediated
310 inflammatory responses between S- and R-variants of *M. canettii* K suggest that bacterial
311 surface remodelling could well have played an important role in the ancestor of the MTBC
312 during adaptation to mammalian hosts. In this respect, the proposed recombination of *pks5*
313 and deletion of *pap* in a common ancestor of the MTBC adds to previously described
314 differences between *M. canettii* and the MTBC, such as the putative loss of vitamin B12
315 production due to the *cobF* deletion^{3,7,9,47,48}, the integration of gene *pe_pgrs33* (*rv1818c*)³, the
316 molecular scars in *pks8/17* and three other gene pairs^{3,7,9}, or the exchange of the exotoxin-
317 encoding domain in CpnT (Rv3903)^{9,49} (Fig. 6). While these reported differences are mainly
318 based on hypotheses formulated during comparative genomics and genome analysis
319 approaches, the virulence differences observed for rough *M. canettii* relative to isogenic LOS-
320 producing smooth *M. canettii* strains now provide first experimental support of our postulated
321 evolutionary model (Fig. 6). Recombination of two ancestral *pks5* genes and consequent
322 remodelling of the bacterial cell surface thus represent key events in the emergence of the
323 professional pandemic pathogen *M. tuberculosis*.

324 **Authors to whom correspondence and requests for materials should be addressed:**

325 Roland Brosch (roland.brosch@pasteur.fr) or Christophe Guilhot
326 (Christophe.Guilhot@ipbs.fr)

327 **Acknowledgements**

328 We thank Torsten Seemann for initial help with NeighborNet analysis, and Hannes Pouseele
329 for help with mapping and SNP analysis. We are also grateful to Ida Rosenkrands and
330 Giovanni Delogu for kindly providing polyclonal anti-SigA antibodies and vector pMV10-25,
331 respectively, and Karim Sébastien for expert assistance in animal care in biosafety-A3
332 facilities. We acknowledge the support by the European Community's grant 260872, the EU-
333 EFPIA Innovative Medicines Initiative (grant 115337), the Agence National de Recherche
334 (ANR-14-JAMR-001-02) and the Fondation pour la Recherche Médicale FRM
335 (DEQ20090515399 and DEQ20130326471). High-throughput sequencing was performed on
336 the Genomics Platform, member of the "France Génomique" consortium (ANR10-INBS-09-
337 08). R.B. is a member of the LabEx consortium IBEID at the Institut Pasteur. F. L-C was
338 supported by the French Region Ile-de- France (Domaine d'Intérêt Majeur Maladies

339 Infectieuses et Emergentes) PhD program. E.C.B. was supported by a stipend from the
340 Pasteur–Paris University (PPU) International PhD program and the Institut Carnot Pasteur
341 Maladies Infectieuses.

342

343 **Author contributions**

344 E.C.B., C.G., L.M. and R.B. designed the study. E.C.B., W.F., F.L.C., and A.P. performed
345 mycobacterial phenotypic assays and/or infection experiments. E.C.B., A.C. and R.B.
346 established genetic constructs. W.M., G.E., F.L., M.D. and C. G. generated and/or analysed
347 mycobacterial lipid and lipooligosaccharide profiles. E.C.B., L.Ma, C.B., M.O., T.P.S. and
348 P.S. generated and/or analysed sequence data. E.C.B and L.Majlessi conducted and analysed
349 immune assays. E.C.B., T.P.S., P.S., C.G. and R.B wrote the manuscript, with comments
350 from all authors.

351

352 **Competing financial interests**

353 P.S. is a consultant for Genoscreen. All other authors declare no competing financial interests.

354

355 **Accession codes**

356 The WGS-generated reads of the *M. canettii* I_{S/R} and K_{S/R} strains were deposited in the
357 European Nucleotide Archive (ENA) under accession number PRJEB11645 (ERP013045).

358

359

360 **Figure legends**

361

362 **Fig. 1.** Comparison of *pks5* genomic region of various mycobacterial strains. (A) *pks5* genetic
363 region of *M. kansasii* ATCC 12478, *M. marinum* M, *M. canettii* A and *M. tuberculosis*
364 H37Rv. Percentages on gray lines represent identity values as defined by ClustalW2 between
365 genes of *M. kansasii*, and *M. marinum* or *M. canettii* A and *M. marinum* or *M. tuberculosis*
366 H37Rv. The red arrows indicate location of primers used for long range PCR of *pks5* gene(s)
367 in *M. canettii* strains I and K, as well as in *M. tuberculosis* H37Rv. (B) Results of long range
368 PCR using above-mentioned primers that bind outside the *pks5* genes. *M. tuberculosis* H37Rv
369 (*Mtb*); *M. canettii* strains: I_S, I_R, K_S and K_R. Note that for strains I_S and I_R unspecific
370 fragments at ~ 12 kb are visible. Data are representative of at least three repetitions. (C)
371 Genetic locus of *pks5* genes in *M. canettii* strains K_S and K_R and potential recombination
372 region in K_R (depicted by black arrows). Percentages on gray lines represent identity values as
373 defined by ClustalW2. (D) Domain organization of the *pks5* genes of *M. canettii* strains K_S

374 and K_R. Domains were predicted according to the organization of *pks5* of *M. tuberculosis*
375 H37Rv⁵⁰ and their respective amino acid positions (AA) are depicted either above or below
376 the particular domains. Sequences of individual domains of *pks5-1* and *pks5-2* were aligned
377 using ClustalW2 and identity values are shown as percentage. Origin of the domains of the
378 recombinant *pks5* of *M. canettii* strain K_R is represented in different nuances of gray (light
379 gray originating from *pks5-2* and dark gray from *pks5-1*; medium gray indicates that domains
380 are identical between *pks5-1* and *pks5-2*). Domain abbreviations: ketosynthase (KS),
381 acyltransferase (AT), dehydratase (DH), enoylreductase (ER), ketoreductase (KR) and acyl-
382 carrier protein (ACP).

383

384 **Figure 2.** Complementation of morphology phenotypes of R variants. (A) Colony
385 morphologies of *M. canettii* strains K_S and I_S and their rough mutants K_R and I_R
386 complemented with the whole *pks5* locus (C9) as well as *M. tuberculosis* H37Rv WT and *M.*
387 *tuberculosis*::C9. Data are representative of at least ten repetitions (plating). Scale bar = 2.5
388 mm. (B) *M. canettii* strains K_S, K_R and K_R::C9 grown in 7H9 medium supplemented with
389 ADC. Data are representative of at least ten repetitions. Scale bar = 5.0 mm. (C) Ziehl-
390 Neelsen staining of *M. canettii* strains K_S, K_R and K_R::C9. Data are representative of 2
391 repetitions. Scale bar = 10 μm.

392

393 **Figure 3.** PFGE and Southern hybridization analyses with PCR-derived probes binding either
394 in a conserved domain of *pks5* (middle panel) or within the *pap* gene (right panel). Genomes
395 of strains were digested with *MfeI*, resulting in either a 20 or a 12 kb fragment (black arrows).
396 For all C9-complemented strains, the probe hybridized twice, with fragments of 20 kb and 12
397 kb confirming the presence of the natural and the vector-integrated *pks5* loci. PFGE gels were
398 run for 16 h with a pulse of 1 s; *M. canettii* A; *M. tuberculosis* H37Rv (*Mtb*); *M. canettii*
399 strains K_S, K_R, K_R::C9; K_R::vector-control; *M. tuberculosis* H37Rv::C9; cosmid C9; M: low-
400 range PFG Marker (NEB). Data are representative of three repetitions.

401

402 **Figure 4.** Deficient LOS production in rough morphotypes. (A) TLC analysis of lipid extracts
403 from various *M. canettii* strains and *M. tuberculosis* H37Rv. Lipid extracts were dissolved in
404 CHCl₃ and run in (CHCl₃:CH₃OH:H₂O, 60:24:2). Glycolipids were visualized by spraying
405 with anthrone, followed by charring. Insert corresponds to an enhanced contrast picture
406 showing a faint blue spot corresponding to LOS in *M. canettii* A. This experiment was
407 performed at least twice with similar results. (B) MALDI-TOF mass spectra of purified LOS

408 from *M. canettii* strains I_S and K_S. Note that the mass peak distribution for the LOS
409 component of strain I was 14 mass-units lower than that observed for K and A. Further
410 MS/MS fragmentation analysis showed successive losses of the O-methyl acylated trehalose
411 and oligosaccharides from the 3 major precursor-ions for strain I, and thus suggests that the
412 difference of 14 mass-units resulted from the presence of a rhamnosyl unit in LOS of strain I,
413 instead of a 2-O-Me-rhamnosyl residue linked to the β -glucosyl unit (L-Rhap- α 1->3-D-Glcp-
414 β 1->3) present in LOS of strains K. (C) TLC analysis (CHCl₃:CH₃OH:H₂O, 60:24:2) of lipid
415 extracts of *M. canettii* strains I_S, I_R, I_R::vector-control, I_R::C9, as well as K_S, K_R, K_R::vector
416 control, K_R::C9 and *M. tuberculosis* H37Rv::C9. This experiment is representative of two
417 experiments performed independently. LOS = lipooligosaccharide. (D) Structure of
418 lipooligosaccharides (LOS) from *M. canettii*. The acyl substituents, primarily 2L-,4L-
419 dimethylhexadecanoate, 2L-,4L-,6L-,8L-tetramethyloctadecanoate, and 2-methyl-3-
420 hydroxyeicosanoate, are at positions 2,3,6 and 3,4,6 of the terminal glucosyl unit²⁹.

421

422 **Figure 5.** Survival of morphotypes in different infection models. (A-B) Intracellular growth
423 of *M. tuberculosis* H37Rv, *M. canettii* strains K_S, K_R, K_R::C9 and K_R::vector-control in
424 differentiated THP-1 macrophages. THP-1 cells were infected with various strains at an MOI
425 of 0.05 (~ 1 bacterium per 20 cells). CFU of intracellular bacteria were determined 3 h and 3,
426 4 and 5 days post infection (pi). The figure shows CFU numbers (A) and fold growth rates
427 (B). Data are represented as means and standard deviation of at least four independent
428 experiments. Significance in difference was determined using Two-way ANOVA (**p* < 0.05,
429 ***p* < 0.001, ****p* < 0.0001). (C) Survival of SCID mice infected with different morphotypes.
430 1 x 10⁶ CFU per mouse of *M. tuberculosis* H37Rv, *M. canettii* strains K_S, K_R or K_R::C9 were
431 IV-injected and survival of mice was monitored. Endpoints were defined as loss of > 20 % of
432 body weight. The initial dose of all strains was comparable with 4.6 x 10⁶ CFU/ml for
433 H37Rv, 3.6 x 10⁶ CFU/ml for K_S, 4.1 x 10⁶ CFU/ml for K_R and 3.3 x 10⁶ CFU/ml for K_R::C9.
434 Data represent one experiment with 10 mice per group. (D) Bacterial load of morphotypes in
435 lungs of infected guinea pigs. Guinea pigs were infected via aerosol route with 2.5x10⁶ CFU.
436 Lungs of infected animals were homogenized at day 1 and day 42 pi and CFU of different
437 morphotypes were determined. Data represent median with interquartile range of CFU at day
438 42 divided by CFU at day 1 of two biological replicates with 4 guinea pigs per group (strains
439 K_S and K_R) or 1 experiment with 4 guinea pigs per group (K_R::C9). Significant difference was
440 observed using Kruskal-Wallis test with Dunn's correction (**p* < 0.05, ***p* < 0.01). (E-F) IL-6
441 and IL-12p40 production in BM-DCs upon infection with different morphotypes. BM-DCs of

442 C57BL/6 WT were infected with Sauton-grown *M. tuberculosis* H37Rv, *M. canettii* strains
443 K_S, K_R or K_R::C9 at an MOI of 1. 24 h pi, levels of IL-6 and IL-12p40 in the cell supernatants
444 were determined by ELISA. Note that a dominant inhibitory effect of LOS on the induction of
445 inflammatory responses was excluded since co-infection of BM-DCs with strains K_S and K_R
446 did not result in less cytokine production than infection with *M. canettii* K_R alone. Data are
447 represented as means and standard deviation of three independent experiments. Significance
448 in difference was determined using Mann Whitney test (**p* < 0.05). (G-H) Differential
449 interaction of S- and R-morphotypes with TLR2. Human TLR2- or TLR4-transfected
450 HEK293 cells were incubated with S- and R-morphotypes at an MOI of 1. At 24 h pi, levels
451 of secreted embryonic alkaline phosphatase reporter gene under the control of NF-κB were
452 measured with a spectrophotometer. PAM3CSK4 (10 μg/ml) and LPS (100 ng/ml) were used
453 as positive controls for TLR2- or TLR4-mediated stimulation, respectively. Data are
454 represented as means and standard deviation of at least three independent experiments.
455 Significance in difference was determined using Mann-Whitney test (****p* < 0.001). n.s. non-
456 stimulated.

457

458 **Figure 6.** Scheme showing supposed molecular key events in mycobacterial evolution from
459 the recombinogenic *M. canettii* strain pool of putative environmental origin, towards
460 professional pathogens of mammalian hosts evolved by clonal expansion of one emerging
461 sublineage. Network phylogeny inferred among eight *M. canettii* strains used in this study,
462 and 46 MTBC strains by NeighborNet analysis based on genome sequence data. Gene names
463 and arrow shown in grey refer to previously described differences between *M. canettii* strains
464 and MTBC members⁹, whereas the *pks5* recombination event is marked by a red arrow.
465 Figure adapted from Bottai et al.¹ and Boritsch et al.⁹.

466

467

468 **METHODS**

469 **Mycobacterial strains and growth conditions**

470 Cloning was performed in LB-grown *Escherichia coli* XL-2 (Stratagene) using hygromycin
471 (200 $\mu\text{g}\cdot\text{ml}^{-1}$) or kanamycin (50 $\mu\text{g}\cdot\text{ml}^{-1}$) selection. MTBC and *M. canettii* strains were
472 grown in Middlebrook 7H9 broth (Becton-Dickinson) containing albumin-dextrose-catalase
473 (ADC) or on Middlebrook 7H11 medium (Becton-Dickinson) containing oleic acid-albumin-
474 dextrose-catalase (OADC) or in Sauton medium (when specified) at 37°C. Hygromycin (50
475 $\mu\text{g}\cdot\text{ml}^{-1}$) was used for mycobacterial selection.

476

477 **Genome analysis of S/R morphotype isolates**

478 Mycobacterial DNA was prepared by standard procedures^{16,17}. After final ethanol
479 precipitation and washing, DNA was resuspended in TE buffer and used for library
480 preparation and Illumina-based genome sequencing. This approach yielded on average 21
481 million (I_S and I_R) and 8 million (K_S and K_R) reads per strain, which were then mapped
482 against the corresponding reference sequences of STB-I (ENA WGS project
483 CAO000000000) and STB-K (NC_019951). Reads were aligned against the reference
484 genomes³ using SHRiMP⁵¹. Alignment maps were visualized with Tablet⁵² and SNPs were
485 called according to coverage sums and variant frequencies. At least 10 reads had to be
486 matched with a substitution frequency > 0.89 to guarantee the detection of high confidence
487 SNPs. Additional mapping and SNP analysis was performed using BioNumerics v7.6
488 software (Applied Maths), using parameters pre-calibrated based on re-sequencing data of
489 reference genomes⁵³.

490

491 **Network phylogenic analysis of *M. canettii* and MTBC strains**

492 Network phylogeny among *M. canettii* and MTBC strains was inferred by NeighborNet
493 analysis, based on pairwise alignments of whole-genome SNP data. Phylogenetic groupings
494 were identified by split decomposition analysis using the SplitsTree4 software⁵⁴.

495

496 **Long-range PCR and *pks5*-sequencing**

497 *pks5* and/or *pap* genes were amplified from chromosomal DNA using Platinum-Taq
498 polymerase (Life Technologies) according to the manufacturer's manual with primers EB-1
499 TTTATTAATCAGGGAAAGGCGACATCGGA and EB-2 TTTTATAACCGCCAAGAC
500 AAACCTTCATC for annealing at 55°C and elongation at 68°C (10 min). Amplicons were
501 Sanger-sequenced after QIAquick (Quiagen) purification, using primers listed in

502 supplementary Table S5. Amplification of *pks5-1* with the last part of *pap* or amplification of
503 *pks5-2* with the first part of *pap* to verify the presence of both *pks5* genes in the various *M.*
504 *canettii* strains was performed using Pwo Polymerase (Roche) and the oligos
505 EB-3 GACGAACTACTAGTCGTTGGTAGCG and EB-4
506 TTTTATAACCGCCAAGACAAACTTCATC, and EB-5
507 TTTCAGGGAAAGGCGACATCGGA and EB-6
508 TTTCGCTACCAACGACTAGTAGTTCGTC, respectively.

509

510 **Complementation of R-variants**

511 R-variants of *M. canettii* strains K and I, as well as *M. tuberculosis* H37Rv and other MTBC
512 members were transformed with the integrating cosmid C9 and H6 spanning the extended or
513 partial *pks5* locus of *M. canettii* strain A. The C9 and H6 clones were selected from a cosmid
514 library that was constructed in pYUB412²⁸ by using partially-digested, agarose-embedded
515 genomic DNA^{55,56} of *M. canettii* reference strain CIPT 140010059 (STB-A). Clone-inserts
516 were PCR-verified using primers binding in vector- or insert-sequences: (T7-F
517 AGGCATGCAAGCTCAGGATA; T7-R GGATCGGTCCAGTAATCGT and T3-F
518 GCAGAAGCACTAGACGATCC; T3-R GCCGCAATTAACCCTCACTA). Transformed,
519 hygromycin-resistant R-variants that exhibited no S-morphology served as vector-controls.
520 Insert-termini sequencing of these latter clones showed partial insert-loss including the *pks5*
521 region, whereas genes encoding MCAN_15411, MCAN_15421 and part of MCAN 15431
522 remained present.

523 For construction of vectors expressing HA-tagged proteins, corresponding genes were
524 amplified with Pwo polymerase (Roche). For the construction of the HA-tagged *pks5-2*
525 expression plasmid, pTTP1b⁵⁷ was cut with *Hind*III (NEB) to remove the kanamycin
526 resistance cassette and blunt ends were generated using Klenow fragment (NEB). A
527 hygromycin resistance cassette was amplified from pAL70⁵⁸ with the oligos AC123
528 ACAGGCCTGTCGTCGAGGTCCACCAA and AC124
529 ACAGGCCTGGATGCCAGGGCCTTTCA, cut with *Stu*I and cloned into the digested vector
530 to generate pAL232. The strong mycobacterial promoter of the gene *hsp60* was amplified
531 from chromosomal DNA of *M. tuberculosis* H37Rv with the oligos *Nhe*I_ *Hind*II_ *hsp60*_F
532 aaaGCTAGCAAGCTTggtgaccacaacgacgcccgtttgatc and *hsp60*_ *Spe*I_ *Eco*RV_ *Xba*I_ R
533 aaaTCTAGAgatatcACTAGTgtcttggccattgccaagtgattcctcc, the amplified product was cut
534 with *Nhe*I and *Xba*I (NEB) and cloned into *Xba*I-digested pAL232 to generate pEB18. The
535 gene *pks5-2* was amplified from chromosomal DNA of *M. canettii* strain K_S with the oligos

536 pks5-2_SpeI_F aaaACTAGTGTGGGTAAGGAGAGAACAAAG and pks5-2_HA_PsiI_R
537 aaaTTATAAttaAGCATAATCAGGAACATCATAACGGATATGAAGGTGCTGCAATGTC
538 GG. The amplified product was cut with *SpeI* and *PsiI* and cloned into *SpeI-EcoRV* digested
539 pEB18. For construction of the HA-tagged *pap* expression system, the plasmid pMV10-25
540 was first cut with *NcoI*, blunt ended using Klenow fragment (NEB) and subsequently cut with
541 *NheI*. The *pap* gene was amplified using the oligos
542 *pap_SpeI_F* aaaACTAGTGTGATCATTGGCGGGGGC and *pap_HA_PsiI_R*
543 aaaTTATAAttaAGCATAATCAGGAACATCATAACGGATAGCTAGATACGCGAACTGC
544 TG. The amplified product was digested with *SpeI* and *PsiI* and cloned into the *NheI*/ blunt
545 end pMV10-25⁵⁹ vector.

546 Whole cell lysates were generated from cultures grown in Middelbrook 7H9 supplemented
547 with ADC to an OD of 0.6-0.8. Cells were disrupted using a TissueLyser II (Quiagen) and
548 Zirkonia/ Silica beads (BioSpec) and passed through 0.2 µm filter units. Proteins were
549 separated on NuPAGE Novex 10% Bis-Tris gels (Invitrogen) for HA-tagged *pap* and
550 NuPAGE Novex 4-12% Bis-Tris gels (Invitrogen) for HA-tagged *pks5-2*. HA-tagged *pap*
551 was blotted on a nitrocellulose membrane using an iBlot Dry Blotting System
552 (LifeTechnologies), while *pks5-2* was blotted on nitrocellulose membranes using a wet
553 transfer system for 2 h at 100 V at 4°C. Membranes were blocked in 5% milk powder in TBS
554 and subsequently incubated with either mouse anti-HA (anti-HA.11; Covance) or rabbit anti-
555 SigA (Statens Serum Institute, Copenhagen, Denmark) primary antibody. Bound antibodies
556 were detected using a horseradish peroxidase-conjugated sheep anti-mouse or donkey anti-
557 rabbit (Amersham ECL) antibody and the chemiluminescent signal was developed with a
558 SuperSignal West Femto Maximum Sensitivity Substrate (Thermo Scientific). Image
559 acquisition was performed with an Azure c300 (Azure Biosystems).

560

561 **Ziehl-Neelsen staining**

562 Mycobacteria were grown to an OD of 0.4, smeared on glass slides and killed at 95°C (1 h).
563 After heat-fixation with 90% ethanol, mycobacteria were stained with carbol-fuchsin and
564 heated (10 min). After washing, glass slides were incubated with sulphuric acid (25%) (2
565 min), washed and incubated with 90% ethanol (5 min), washed and counter-stained with
566 methylene blue (2 min).

567

568 **PFGE and Southern Blot hybridization**

569 Genomic DNA in agarose-plugs, prepared as described⁵⁵, was *MfeI*-digested, separated by
570 pulsed-field gel electrophoresis (Biorad CHEF II, pulse 1 s for 16 h at 6 V·cm⁻¹) and
571 transferred onto Hybond-C-Extra nitrocellulose (GE), as described⁵⁵. Hybridization was
572 performed with [α -³²P]dCTP-labeled PCR-probes at 68°C in 6xSSC/ 0,5% SDS/ 0.01 M
573 EDTA/ 5xDenhardt's solution/ 100 mg·ml⁻¹salmon-sperm DNA. After washing, membranes
574 were exposed to phosphorimager screens, which were scanned in a STORM phosphorimager.
575 Probes were amplified from *M. tuberculosis* DNA using *pks5* primers (*pks5*-F
576 GTTGTGGGAGGCGTTGCT; *pks5*-R GAAACGTCGAACGCATGAC) or from *M. canettii*
577 K_s using *pap* primers (*pap*-F CTCGATTATTACGGCTGGT; *pap*-R
578 CGTATAGCCCGGTGATCAAC).

579

580 **Extraction and analysis of lipooligosaccharides**

581 Mycobacterial cells obtained from 7H9-grown cultures were exposed to CHCl₃/CH₃OH (1:2,
582 v/v) for 48h to kill bacteria. Lipids were extracted following previously described
583 protocols^{14,21} and separated by TLC. Finally, glycolipids were visualized by spraying the
584 plates with a 0.2% anthrone solution (w/v) in concentrated H₂SO₄, followed by heating. The
585 previously described LOS of *M. canettii* strain CIPT 140010059 was used as standard²⁹.
586 Crude lipid extracts were subjected to chromatography on a Sep-Pak Florisil cartridge and
587 eluted at various concentrations of CH₃OH (0, 5, 10, 15, 20, 30%) in CHCl₃. Each fraction
588 was analyzed by TLC on Silica Gel G60 using CHCl₃/CH₃OH/H₂O (30:12:1, v/v/v) as solvent
589 and glycolipids were visualized as described above.

590 MALDI-TOF/TOF-MS and MS/MS analyses were conducted in the positive
591 ionization and reflectron mode by accumulating 10 spectra of 250 laser shots, using the 5800
592 MALDI TOF/TOF Analyser (Applied Biosystems/Absciex) equipped with a Nd:Yag laser
593 (349nm). For MS and MS/MS data acquisitions, uniform, continuous, and random stage
594 motion was selected at a fixed laser intensity of 4000 (instrument-specific units) and 400 Hz
595 pulse rate and 6000 (instrument-specific units) and 1000Hz, respectively. For MS/MS data
596 acquisition, the fragmentation of selected precursor-ions was performed at collision energy of
597 1 kV. Lipid samples were dissolved in chloroform and spotted onto the target plate as 0.5 μ l
598 droplets, followed by the addition of 0.5 μ l matrix solution (10 mg of 2,5-dihydroxybenzoic
599 acid [Sigma-Aldrich]/ml in CHCl₃/CH₃OH, 1/1 [vol/vol]). Samples were allowed to crystallize
600 at room temperature. Spectra were externally calibrated using lipid standards.

601 Alkaline hydrolysis of purified LOS and total extractable lipids from the various
602 strains was performed with 1M sodium methanolate for 1h at 37°C. After neutralization with

603 glacial acetic acid, the mixture was dried under stream of nitrogen and lipids were extracted
604 with diethyl ether and washed twice with water. The resulting fatty acid methyl esters were
605 converted to trimethylsilyl (TMS) derivatives, using a mixture of
606 pyridine/hexamethyldisilazane/trimethylchlorosilane (6:4:2, v/v/v).

607 GC-MS analyses were performed using a Thermo TraceGCultra chromatograph
608 coupled with an ISQ mass spectrometer. Chromatographic separations of the TMS derivatives
609 of the fatty acid methyl esters were obtained using an Inferno ZB5HT column of 15m. Helium
610 was the carrier gas at constant flow rate of 1.2mL min⁻¹. The oven temperature program was
611 started at 120°C, ramped to 380°C at 10°C/min (with final isothermal step of 5min at 380°C).
612 The temperature of the injector was 220°C and injection of 1µl of samples in petroleum ether
613 was performed in a split mode (ratio of 20:1). EI mass spectra were recorded using electron
614 energy of 70eV from 60 to 600 with a transfer line maintained at 275°C.

615 To visualize various polyketide-derive lipids, including acyl-trehaloses such
616 diacyltrehaloses (DAT), polyacyltrehaloses (PAT), sulfolipids (SL), phenolic glycolipids
617 (PGL) or lipooligosaccharides (LOS) from different *M. canettii* strains metabolic labelling
618 with ¹⁴C propionate was used. For this TLC analysis, *M. canettii* strains were grown to the
619 exponential phase in 10 mL 7H9 liquid medium supplemented with ADC and 0.05% Tween
620 80 and labelled by incubation with 0.4 µCi.ml⁻¹ [1-¹⁴C] propionate for 24 h. The TLC plates
621 were run in CHCl₃/CH₃OH/H₂O (60/16/2) for DAT and SL and CHCl₃/CH₃OH (99/1) for
622 PAT. Labelled lipids were visualized with a Typhoon PhosphorImager (Amersham
623 Biosciences).

624

625 **Macrophage infections**

626 THP-1 (TIB-202D) human monocyte-like cells were purchased from ATCC, directly
627 amplified and stocked in liquid nitrogen. Only low passage cells (passage number <11) were
628 used in the experiments. The purchased THP-1 cell line has been authenticated and tested for
629 microbial contaminants, including mycoplasma, by ATCC. For the experiments, THP-1 were
630 cultivated in RPMI 1640, GlutaMAX (Life Technologies) containing 10 % heat-inactivated
631 fetal bovine serum (Life Technologies), seeded at a density of 7.5x10⁴ cells per well in 96
632 well plates and differentiated into macrophages through incubation with 50 mM PMA for 3
633 days. For infection, bacteria grown in Sauton medium without shaking were sonicated, added
634 to the macrophages at an MOI of 0.05, (~ 1 bacterium per 20 THP-1 cells) and incubated for 2
635 h. Sauton medium was used, as it allows the production of more complex polar lipids¹⁸. After
636 phagocytosis, 0.1 mg·ml⁻¹ amikacin was added for 1 h to remove extracellular bacteria and

637 cells were incubated for up to 6 days at 37°C and 5% CO₂. At various time points
638 macrophages were lysed with 0.1% Triton-X100 in PBS and lysates plated in serial dilutions
639 on 7H11+OADC plates to determine intracellular survival of bacteria in CFU. Experiments
640 were performed as at least four biological replicates, each done in triplicate (technical
641 replicates).

642 Additional infection experiments were conducted using Raw murine macrophages as
643 well as Human monocyte-derived macrophages (hMDMs). Raw cells were cultivated in
644 RPMI 1640 Medium, GlutaMAX (Gibco, Life Technologies) supplemented with 5 % heat-
645 inactivated fetal bovine serum (Gibco, Life Technologies) and seeded one day before
646 infection. In parallel, hMDMs were obtained from buffy coats by centrifugation of blood from
647 healthy human donors in lymphocyte separation medium (Eurobio) and further isolation of
648 CD14⁺ monocytes from the mononuclear cell fraction using CD14 microbeads (Miltenyi
649 Biotec). Monocytes were differentiated into macrophages in the presence of rhM-CSF (50
650 ng/ml; R&D Systems). At the day of infection mycobacterial strains grown in Sauton medium
651 without shaking were sonicated, added to the macrophages at a MOI of 1:20, and incubated
652 for 2 hrs at 37°C and 5% CO₂. After phagocytosis, infected macrophages were incubated with
653 0.1 mg·ml⁻¹ amikacin for 1 h to remove extracellular bacteria and finally incubated for 6 days
654 in new RPMI supplemented with 10 % FBS for hMDMs and 1% for Raw cells at 37°C and 5
655 % CO₂. At selected time points macrophages were lysed with 0.1 % Triton-X100 in PBS and
656 bacteria were plated in serial dilutions on 7H11 plates supplemented with OADC to determine
657 CFU counts. Buffy coats were obtained from healthy donors after informed consent
658 (Etablissement Français du Sang). Three biological replicates were performed, each done in
659 triplicate (technical replicates).

660

661 **Animal infection studies**

662 Six-week-old female SCID mice (Charles River) were infected intravenously with 200 µl of
663 5x10⁶ bacteria/mouse and survival of mice was monitored. Humane endpoints were defined
664 as loss of > 20 % of body-weight. The experiment was performed once, using 10 mice per
665 strain (technical replicates). In a second well-established mycobacterial infection model, five
666 to six week-old female guinea pigs (Hartley; Charles River) were aerosol-infected using 5 ml
667 of a suspension containing 5x10⁵ bacteria·ml⁻¹. Six weeks post-infection, animals were killed
668 and organs homogenized using a gentleMACS Dissociator (Miltenyi Biotec) and
669 gentleMACS M tubes. Bacterial loads in organs were determined by plating serial dilutions of
670 organ homogenates on solid medium. The number of animals included in the experiments

671 (sample size choice) was determined by taking into account the rule of 3Rs (replacement,
672 reduction, refinement) and statistical requirements. As regards randomization and blinding,
673 CFU counts were recorded in parallel by different investigators.

674

675 **Cytokine and chemokine assays and HEK-Blue cell reporter assay**

676 ELISA and ProcartaPlex Luminex immunoassay from culture supernatants of infected BM-
677 DCs was performed as previously described⁶⁰, and/or according to the manufacturer's
678 instructions (ProcartaPlex Luminex Immunoassay). mAbs specific to IL-12p40 and IL-6 were
679 from BD Biosciences. Reagents for quantitative ProcartaPlex Luminex immunoassay were
680 from affymetrix eBioscience. ELISA experiments were performed as three biological
681 replicates, while Luminex analyses were performed as two independent biological replicates,
682 each done in duplicate. Signal acquisition was performed on pooled duplicates.

683 HEK-TLR2 and HEK-TLR4 cells (InvivoGen) were grown in DMEM medium (Gibco Life
684 Technologies) supplemented with 10% FBS, 100 $\mu\text{g}\cdot\text{ml}^{-1}$ Normocin and 1X HEK-Blue
685 Selection. TLR stimulation assay was performed according to the manufacturer's protocol. 10
686 $\mu\text{g}\cdot\text{ml}^{-1}$ PAM3CSK4 served as positive control for HEK-TLR2 and 100 $\text{ng}\cdot\text{ml}^{-1}$ LPS as
687 positive control for HEK-TLR4. Experiments were performed as at least three biological
688 replicates.

689

690 **Compliance with regulations on animal welfare and ethics**

691 Animal studies were performed in agreement with European and French guidelines (Directive
692 86/609/CEE and Decree 87-848 of 19 October 1987) after approval by the Institut Pasteur
693 Safety Committee (Protocol 11.245) and local ethical committees (CNREEA 2012-0061;
694 CETEA 2013-0036).

695

696 **References:**

- 697 1 Bottai, D., Stinear, T. P., Supply, P. & Brosch, R. Mycobacterial Pathogenomics and
698 Evolution *Microbiology Spectrum* **2**, MGM2-0025-2013 (2014).
- 699 2 Le Chevalier, F., Cascioferro, A., Majlessi, L., Herrmann, J. L. & Brosch, R.
700 *Mycobacterium tuberculosis* evolutionary pathogenesis and its putative impact on
701 drug development. *Future Microbiol.* **9:969-85.**, (2014).
- 702 3 Supply, P. *et al.* Genomic analysis of smooth tubercle bacilli provides insights into
703 ancestry and pathoadaptation of *Mycobacterium tuberculosis*. *Nat Genet* **45**, 172-179
704 (2013).
- 705 4 van Soolingen, D. *et al.* A novel pathogenic taxon of the *Mycobacterium tuberculosis*
706 complex, Canetti: characterization of an exceptional isolate from Africa. *Int J Syst*
707 *Bacteriol* **47**, 1236-1245. (1997).

708 5 Gutierrez, M. C. *et al.* Ancient origin and gene mosaicism of the progenitor of
709 Mycobacterium tuberculosis. *PLoS Pathog.* **1**, e5.

710 6 Koeck, J. L. *et al.* Clinical characteristics of the smooth tubercle bacilli
711 'Mycobacterium canettii' infection suggest the existence of an environmental reservoir.
712 *Clin Microbiol Infect* **17**, 1013-1019 (2011).

713 7 Blouin, Y. *et al.* Progenitor "Mycobacterium canettii" Clone Responsible for Lymph
714 Node Tuberculosis Epidemic, Djibouti. *Emerg Infect Dis* **20**, 21-28, (2014).

715 8 Dormans, J. *et al.* Correlation of virulence, lung pathology, bacterial load and delayed
716 type hypersensitivity responses after infection with different *Mycobacterium*
717 *tuberculosis* genotypes in a BALB/c mouse model. *Clin Exp Immunol.* **137**, 460-468.
718 (2004).

719 9 Boritsch, E. C. *et al.* A glimpse into the past and predictions for the future: the
720 molecular evolution of the tuberculosis agent. *Mol Microbiol.* **93**, 835-852. (2014).

721 10 Panas, M. W. *et al.* Noncanonical SMC protein in *Mycobacterium smegmatis* restricts
722 maintenance of *Mycobacterium fortuitum* plasmids. *Proc Natl Acad Sci U S A.* **111**,
723 13264-13271. (2014).

724 11 Kansal, R. G., Gomez-Flores, R. & Mehta, R. T. Change in colony morphology
725 influences the virulence as well as the biochemical properties of the *Mycobacterium*
726 *avium* complex. *Microb Pathog* **25**, 203-214, (1998).

727 12 Catherinot, E. *et al.* Hypervirulence of a rough variant of the *Mycobacterium*
728 *abscessus* type strain. *Infect Immun* **75**, 1055-1058, (2007).

729 13 Belisle, J. T. & Brennan, P. J. Chemical basis of rough and smooth variation in
730 mycobacteria. *J Bacteriol.* **171**, 3465-3470. (1989).

731 14 van der Woude, A. D. *et al.* Unexpected link between lipooligosaccharide biosynthesis
732 and surface protein release in *Mycobacterium marinum*. *J Biol Chem* **287**, 20417-
733 20429, (2012).

734 15 Barrow, W. W. & Brennan, P. J. Isolation in high frequency of rough variants of
735 *Mycobacterium intracellulare* lacking C-mycoside glycopeptidolipid antigens. *J*
736 *Bacteriol.* **150**, 381-384. (1982).

737 16 Howard, S. T. *et al.* Spontaneous reversion of *Mycobacterium abscessus* from a
738 smooth to a rough morphotype is associated with reduced expression of
739 glycopeptidolipid and reacquisition of an invasive phenotype. *Microbiology* **152**,
740 1581-1590, (2006).

741 17 Pawlik, A. *et al.* Identification and characterization of the genetic changes responsible
742 for the characteristic smooth-to-rough morphotype alterations of clinically persistent
743 *Mycobacterium abscessus*. *Mol. Microbiol.* **90**, 612-629. (2013).

744 18 Burguiere, A. *et al.* LosA, a key glycosyltransferase involved in the biosynthesis of a
745 novel family of glycosylated acyltrehalose lipooligosaccharides from *Mycobacterium*
746 *marinum*. *J Biol Chem.* **280**, 42124-42133. (2005).

747 19 Ren, H. *et al.* Identification of the lipooligosaccharide biosynthetic gene cluster from
748 *Mycobacterium marinum*. *Mol Microbiol* **63**, 1345-1359 (2007).

749 20 Lemassu, A., Levy-Frebault, V. V., Laneelle, M. A. & Daffe, M. Lack of correlation
750 between colony morphology and lipooligosaccharide content in the *Mycobacterium*
751 *tuberculosis* complex. *J Gen Microbiol.* **138**, 1535-1541. (1992).

752 21 Etienne, G. *et al.* Identification of the polyketide synthase involved in the biosynthesis
753 of the surface-exposed lipooligosaccharides in mycobacteria. *J Bacteriol* **191**, 2613-
754 2621 (2009).

755 22 Nataraj, V. *et al.* MKAN27435 is required for the biosynthesis of higher subclasses of
756 lipooligosaccharides in *Mycobacterium kansasii*. *PLoS One.* **10**, e0122804. (2015).

- 757 23 Minnikin, D. E. *et al.* in *Tuberculosis - Expanding Knowledge* (ed W. Ribon) Ch. 7,
758 (InTech, 2015).
- 759 24 Stinear, T. P. *et al.* Insights from the complete genome sequence of *Mycobacterium*
760 *marinum* on the evolution of *Mycobacterium tuberculosis*. *Genome Res* **18**, 729-741.
761 (2008).
- 762 25 Wang, J. *et al.* Insights on the Emergence of *Mycobacterium tuberculosis* from the
763 Analysis of *Mycobacterium kansasii*. *Genome Biol Evol.* **7**, 856-870. doi:
764 810.1093/gbe/evv1035. (2015).
- 765 26 Quadri, L. E. Biosynthesis of mycobacterial lipids by polyketide synthases and
766 beyond. *Crit Rev Biochem Mol Biol.* **49**, 179-211. (2014).
- 767 27 Rousseau, C. *et al.* Virulence attenuation of two Mas-like polyketide synthase mutants
768 of *Mycobacterium tuberculosis*. *Microbiology.* **149**, 1837-1847. (2003).
- 769 28 Bange, F. C., Collins, F. M. & Jacobs, W. R., Jr. Survival of mice infected with
770 *Mycobacterium smegmatis* containing large DNA fragments from *Mycobacterium*
771 *tuberculosis*. *Tuber Lung Dis* **79**, 171-180. (1999).
- 772 29 Daffe, M., McNeil, M. & Brennan, P. J. Novel type-specific lipooligosaccharides from
773 *Mycobacterium tuberculosis*. *Biochemistry.* **30**, 378-388. (1991).
- 774 30 Angala, S. K., Belardinelli, J. M., Huc-Claustre, E., Wheat, W. H. & Jackson, M. The
775 cell envelope glycoconjugates of *Mycobacterium tuberculosis*. *Crit Rev Biochem Mol*
776 *Biol.* **49**, 361-399. (2014).
- 777 31 Onwueme, K. C., Ferreras, J. A., Buglino, J., Lima, C. D. & Quadri, L. E.
778 Mycobacterial polyketide-associated proteins are acyltransferases: proof of principle
779 with *Mycobacterium tuberculosis* PapA5. *Proc Natl Acad Sci U S A.* **101**, 4608-4613.
780 (2004).
- 781 32 Bhatt, K., Gurcha, S. S., Bhatt, A., Besra, G. S. & Jacobs, W. R., Jr. Two polyketide-
782 synthase-associated acyltransferases are required for sulfolipid biosynthesis in
783 *Mycobacterium tuberculosis*. *Microbiology.* **153**, 513-520. (2007).
- 784 33 Bottai, D. *et al.* Increased protective efficacy of recombinant BCG strains expressing
785 virulence-neutral proteins of the ESX-1 secretion system. *Vaccine.* **33**, 2710-2718.
786 (2015).
- 787 34 Rhoades, E. R. *et al.* *Mycobacterium abscessus* Glycopeptidolipids mask underlying
788 cell wall phosphatidyl-myo-inositol mannosides blocking induction of human
789 macrophage TNF-alpha by preventing interaction with TLR2. *J Immunol* **183**, 1997-
790 2007, (2009).
- 791 35 Roux, A. L. *et al.* Overexpression of proinflammatory TLR-2-signalling lipoproteins
792 in hypervirulent mycobacterial variants. *Cell Microbiol* **13**, 692-704, (2011).
- 793 36 Robinson, R. T., Orme, I. M. & Cooper, A. M. The onset of adaptive immunity in the
794 mouse model of tuberculosis and the factors that compromise its expression. *Immunol*
795 *Rev.* **264**, 46-59. (2015).
- 796 37 Achtman, M. Insights from genomic comparisons of genetically monomorphic
797 bacterial pathogens. *Philos Trans R Soc Lond B Biol Sci* **367**, 860-867 (2012).
- 798 38 Portevin, D. *et al.* A polyketide synthase catalyzes the last condensation step of
799 mycolic acid biosynthesis in mycobacteria and related organisms. *Proc Natl Acad Sci*
800 *U S A* **101**, 314-319. (2004).
- 801 39 Constant, P. *et al.* Role of the *pks15/l* gene in the biosynthesis of phenolglycolipids in
802 the *Mycobacterium tuberculosis* complex. Evidence that all strains synthesize
803 glycosylated *p*-hydroxybenzoic methyl esters and that strains devoid of
804 phenolglycolipids harbor a frameshift mutation in the *pks15/l* gene. *J Biol Chem* **277**,
805 38148-38158, (2002).

- 806 40 Matsunaga, I. *et al.* *Mycobacterium tuberculosis pks12* produces a novel polyketide
807 presented by CD1c to T cells. *J Exp Med.* **200**, 1559-1569. (2004).
- 808 41 Rombouts, Y. *et al.* Fatty acyl chains of *Mycobacterium marinum*
809 lipooligosaccharides: structure, localization and acylation by PapA4 (MMAR_2343)
810 protein. *J Biol Chem.* **286**, 33678-33688. (2011).
- 811 42 Alibaud, L. *et al.* Increased phagocytosis of *Mycobacterium marinum* mutants
812 defective in lipooligosaccharide production: a structure-activity relationship study. *J*
813 *Biol Chem.* **289**, 215-228. (2014).
- 814 43 Eckstein, T. M., Inamine, J. M., Lambert, M. L. & Belisle, J. T. A genetic mechanism
815 for deletion of the *ser2* gene cluster and formation of rough morphological variants of
816 *Mycobacterium avium*. *J Bacteriol* **182**, 6177-6182 (2000).
- 817 44 Ortalo-Magne, A. *et al.* Identification of the surface-exposed lipids on the cell
818 envelopes of *Mycobacterium tuberculosis* and other mycobacterial species. *J Bacteriol*
819 **178**, 456-461 (1996).
- 820 45 Mortaz, E. *et al.* Interaction of Pattern Recognition Receptors with *Mycobacterium*
821 *tuberculosis*. *J Clin Immunol* **14**, 14 (2014).
- 822 46 Cambier, C. J. *et al.* Mycobacteria manipulate macrophage recruitment through
823 coordinated use of membrane lipids. *Nature.* **505**, 218-222. (2014).
- 824 47 Gopinath, K., Moosa, A., Mizrahi, V. & Warner, D. F. Vitamin B(12) metabolism in
825 *Mycobacterium tuberculosis*. *Future Microbiol* **8**, 1405-1418 (2013).
- 826 48 Young, D. B., Comas, I. & de Carvalho, L. P. Phylogenetic analysis of vitamin B12-
827 related metabolism in *Mycobacterium tuberculosis*. *Front Mol Biosci.* **2**, 6. (2015)
- 828 49 Danilchanka, O. *et al.* An outer membrane channel protein of *Mycobacterium*
829 *tuberculosis* with exotoxin activity. *Proc Natl Acad Sci U S A.* **111**, 6750-6755.
830 (2014).
- 831 50 Delahay *et al.* The coiled-coil domain of EspA is essential for the assembly of the type
832 III secretion translocon on the surface of enteropathogenic *Escherichia coli*. *J Biol*
833 *Chem.* **274**, 35969-35974.

834

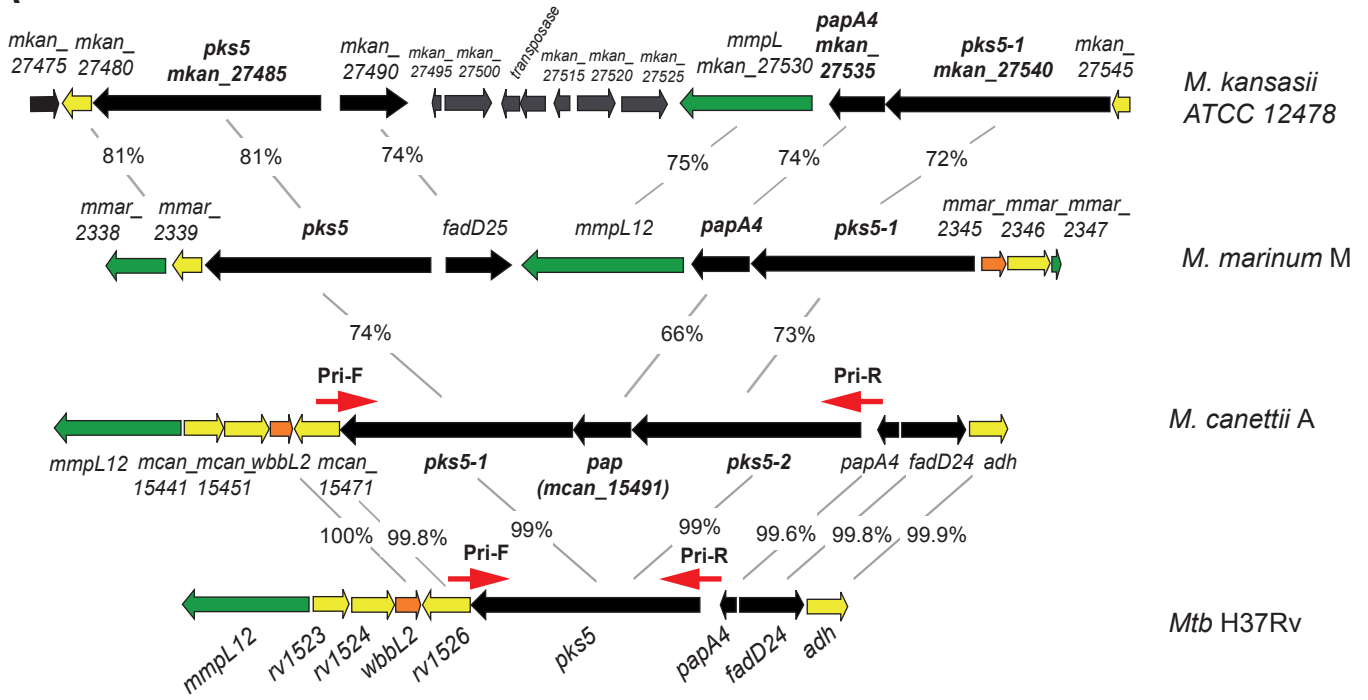
835 **References Methods**

836

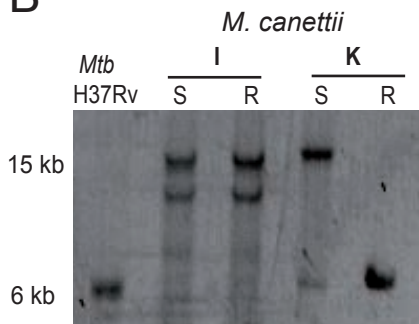
- 837 51 David, M., Dzamba, M., Lister, D., Ilie, L. & Brudno, M. SHRiMP2: sensitive yet
838 practical SHort Read Mapping. *Bioinformatics.* **27**, 1011-1012. (2011).
- 839 52 Milne, I. *et al.* Using Tablet for visual exploration of second-generation sequencing
840 data. *Brief Bioinform.* **14**, 193-202. (2013).
- 841 53 Pouseele, H. & Supply, P. Accurate whole-genome sequencing-based epidemiological
842 surveillance of mycobacterium tuberculosis. *Methods in Microbiology.*
843 doi:10.1016/bs.mim.2015.04.001 (2015).
- 844 54 Huson, D. H. & Bryant, D. Application of phylogenetic networks in evolutionary
845 studies. *Mol Biol Evol* **23**, 254-267 (2006).
- 846 55 Brosch, R. *et al.* Comparative genomics uncovers large tandem chromosomal
847 duplications in *Mycobacterium bovis* BCG Pasteur. *Yeast* **17**, 111-123. (2000).
- 848 56 Brosch, R. *et al.* Use of a *Mycobacterium tuberculosis* H37Rv bacterial artificial
849 chromosome library for genome mapping, sequencing, and comparative genomics.
850 *Infect Immun* **66**, 2221-2229 (1998).
- 851 57 Pham, T. T., Jacobs-Sera, D., Pedulla, M. L., Hendrix, R. W. & Hatfull, G. F.
852 Comparative genomic analysis of mycobacteriophage Tweety: evolutionary insights
853 and construction of compatible site-specific integration vectors for mycobacteria.
854 *Microbiology.* **153**, 2711-2723 (2007).

855 58 Cascioferro, A. *et al.* Xer site-specific recombination, an efficient tool to introduce
856 unmarked deletions into mycobacteria. *Appl Environ Microbiol* **76**, 5312-5316 (2010).
857 59 Delogu, G. *et al.* Rv1818c-encoded PE_PGRS protein of *Mycobacterium tuberculosis*
858 is surface exposed and influences bacterial cell structure. *Mol Microbiol* **52**, 725-733
859 (2004).
860 60 Majlessi, L. *et al.* Influence of ESAT-6 Secretion System 1 (RD1) of *Mycobacterium*
861 *tuberculosis* on the Interaction between Mycobacteria and the Host Immune System. *J*
862 *Immunol* **174**, 3570-3579 (2005).
863

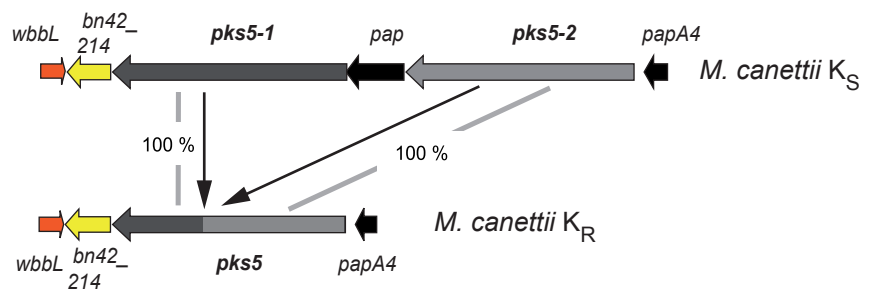
A



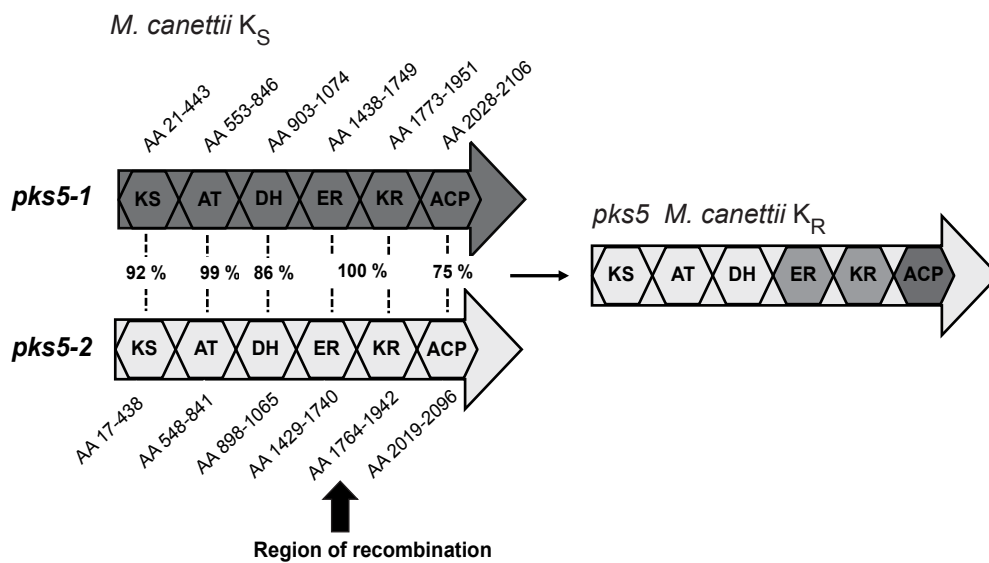
B

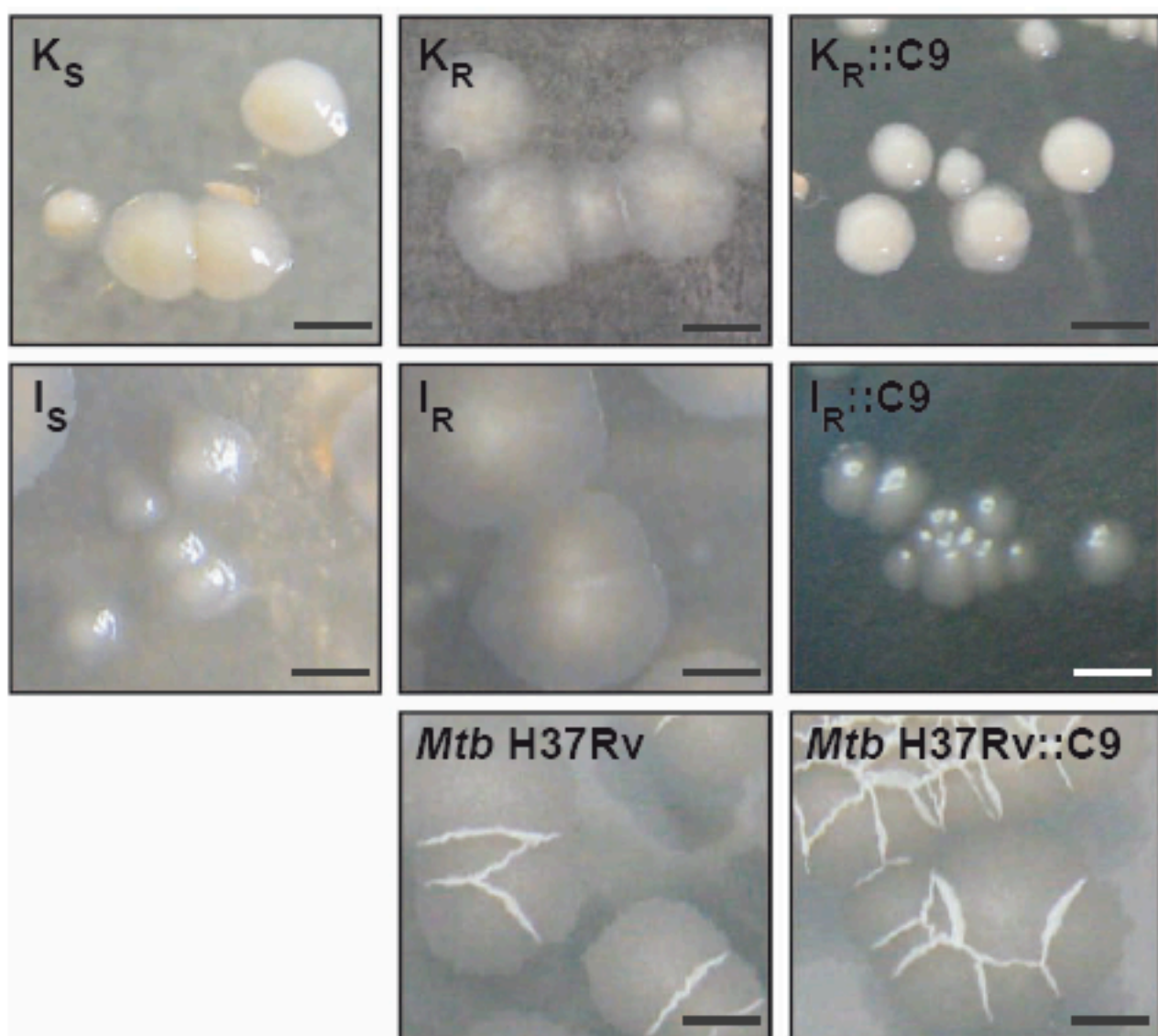
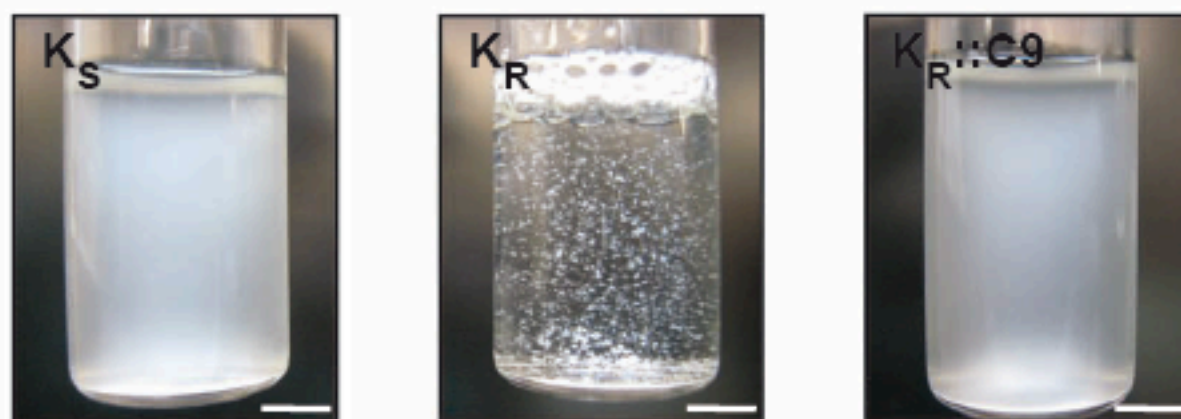


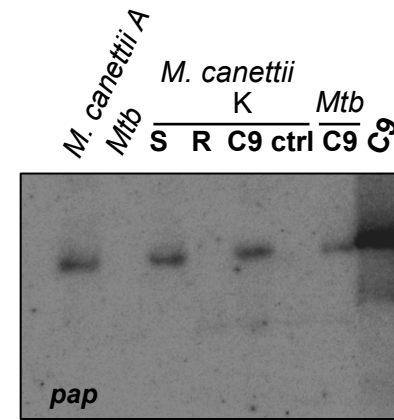
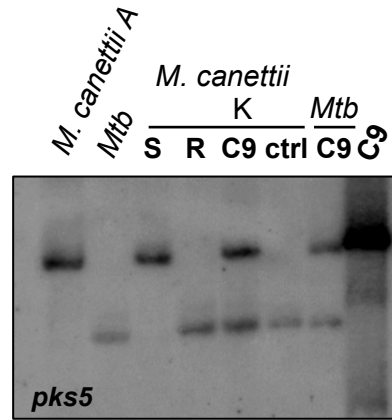
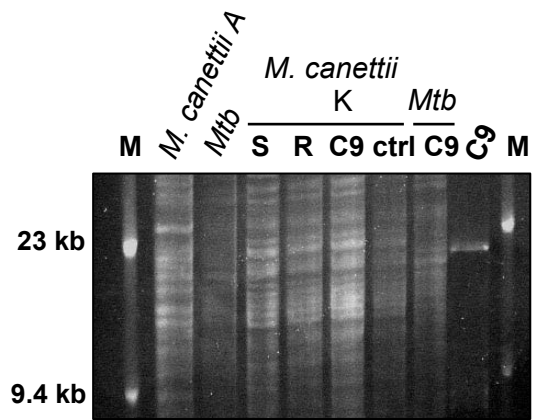
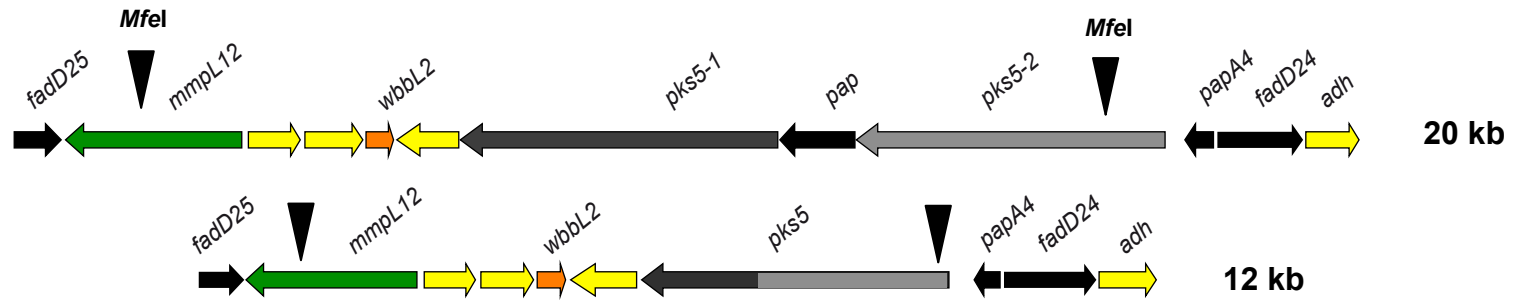
C

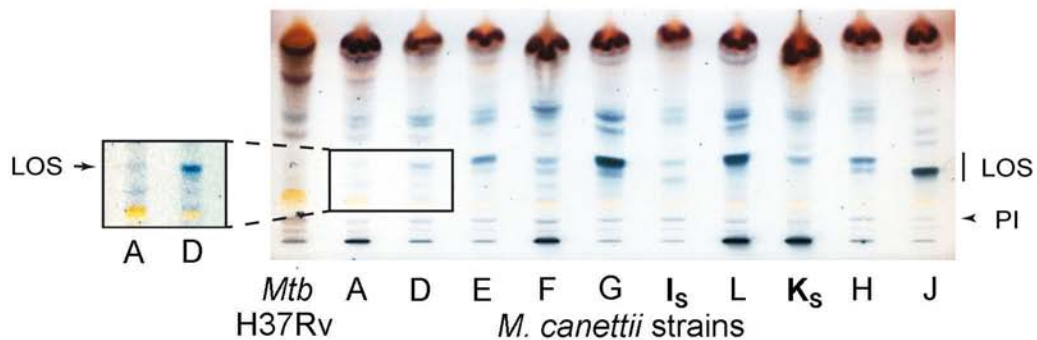
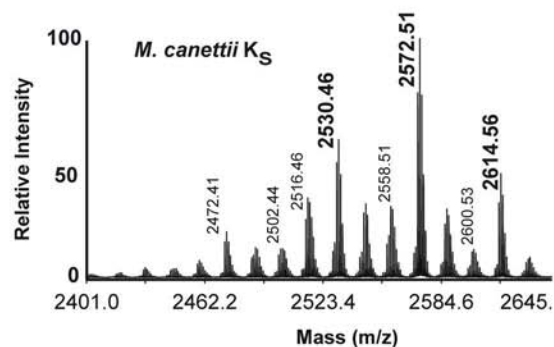
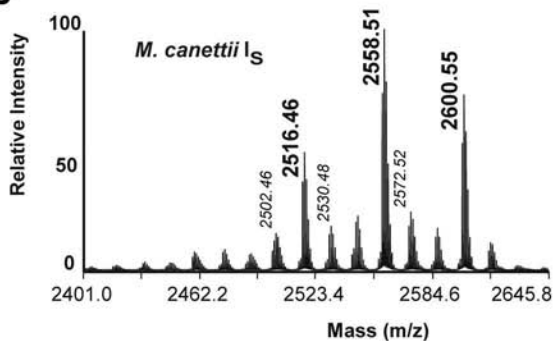
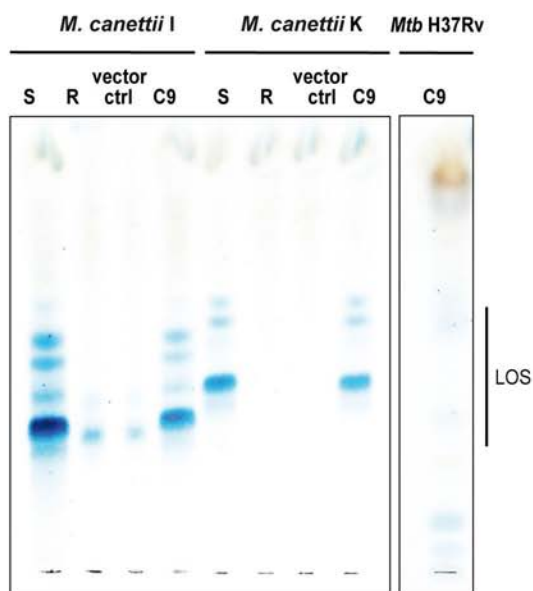


D



A*M. canettii***B****C**



A**B****C****D**